Advances in Materials, Manufacturing, and Repair for Power Plants:
Proceedings from the Tenth International Conference
October 15–18, 2024, Bonita Springs Florida, USA
https://doi.org/10.31399/asm.cp.epri2024p0365

MICROSTRUCTURE OF MODIFIED 9CR-1MO STEEL MANUFACTURED VIA LASER POWDER BED FUSION

Tomotaka Hatakeyama, Kota Sawada, Masaru Suzuki, Makoto Watanabe
National Institute for Materials Science, Tsukuba, Ibaraki, Japan

ABSTRACT

Modified 9Cr-1Mo steel was manufactured via laser powder bed fusion (LPBF) using gas atomized powders under various building conditions. Dense samples were obtained at an energy density of 111–125 J/mm^3. As-built samples were subjected to a normalization and tempering heat treatments. The microstructure of the as-built sample exhibits a duplex structure, comprising coarse columnar δ-ferrite grains and fine martensite grains. In addition, a small amount of retained austenite phase was observed at the interface between δ-ferrite and martensite. The formation of δ-ferrite is attributed to the extremely rapid solidification that occurs during the LPBF process, while martensite is obtained through the phase transformation because of the thermal cycles experienced during the process. The area fraction of δ-ferrite and martensite can be controlled by adjusting the LPBF parameters. Typical as-built microstructure morphology characterized by the columnar δ-ferrite was eliminated after the heat treatments, resulting in a tempered martensitic microstructure that is identical with that obtained through the conventional process. However, an increase in prior austenite grain size was observed when the area fraction of δ-ferrite in the as-built condition was high, due to faster phase transformation kinetics of martensite than that of δ-ferrite during the normalization. This suggests that the prior austenite grain size can be controlled by optimizing the area fraction of δ-ferrite and martensite in the as-built microstructure.

INTRODUCTION

Additive manufacturing technology has received considerable attentions because of its outstanding superiority in the net-shaping of complex-shaped products, which can save production time and cost. Laser powder bed fusion (LPBF) is a common additive manufacturing technology. Laser melting of the selected area of the powder bed and layer-by-layer manufacturing provide a specific solidification microstructure resulting from the melt-pool geometry and laser scan strategy. Therefore, understanding of the microstructure formation mechanism is important because mechanical properties are influenced by the microstructure.

Modified 9Cr-1Mo steel is a ferritic heat-resistant steel widely used in boiler tubes and pipes in thermal power plants because of its excellent creep strength [1]. The typical microstructure of modified 9Cr-1Mo steel is tempered martensite, which is controlled by normalizing and tempering heat treatments. In addition, additively manufactured modified 9Cr-1Mo steel is expected to be applied in the components of next-generation nuclear reactors [2].

During the LPBF process, the complex microstructure development of the modified 9Cr-1Mo steel is expected because of the repetition of melting and solidification and the accompanying martensite transformation. This study was motivated to reveal the microstructure formation mechanism of modified 9Cr-1Mo steel during LPBF. In addition, the effect of heat treatments on the microstructure of the LPBF-manufactured modified 9Cr-1Mo steel was investigated.

EXPERIMENTAL PROCEDURES

Powder which chemical composition satisfies the specification of ASME SA213/SA213M Grade T91 Type 1 [3] was prepared by gas atomization. The specification of ASME Grade T91 steel and chemical composition of the powder are summarized in Table 1. The average powder size (d_{50}) was 40.9 μm. 10×10×15 mm^3 specimens were additively manufactured via laser powder bed fusion using the SLM280 3D printer (SLM Solutions). Laser power (P), scan speed (v), rotation angle of laser scan in each layer, hatch distance (h), layer thickness (t), and energy density ($E = P/vht$) used in this study are summarized in Table 2.

Table 1: Specification of ASME Grade T91 steel [3] *and Chemical composition of the gas atomized powder (mass%)*

	C	Si	Mn	P	S	Ni	Cr
Specification	0.07-0.14	0.20-0.50	0.30-0.60	≦0.020	≦0.010	≦0.40	8.0-9.5
Powder	0.10	0.38	0.47	0.006	0.002	0.06	8.8

Mo	Al	Ti	V	Nb	Zr	Fe	N
0.85-1.05	≦0.02	≦0.01	0.18-0.25	0.06-0.10	≦0.01	-	0.030-0.070
0.95	<0.01	<0.01	0.25	0.09	<0.01	Bal.	0.06

Table 2: LPBF parameters performed in this study.

Laser power, P [W]	Scan speed, v [mm/s]	Rotation angle [degree]	Hatch distance, h [mm]	Layer thickness, t [mm]	Energy density, E [J/mm^3]
100	400	67	0.1	0.03	83.3
		90			
	600	67			55.6
		90			
	800	67			41.7
		90			
200	400	67			166.7
		90			
	600	67			111.1
		90			
	800	67			83.3
		90			
300	400	67			250.0
		90			
	600	67			166.7
		90			
	800	67			125.0
		90			

As-built sample was normalized at 1323 K for 30 minutes followed by tempering at 1053 K for 60 minutes. Microstructure of as-built and normalized + tempered (NT) samples were characterized

by optical microscopy (OM), scanning electron microscopy (SEM), and electron backscattered diffraction (SEM-EBSD). Vickers hardness of the samples was measured at room temperature with a load of 10 kgf.

RESULTS AND DISCUSSION

Figure 1(a) shows the relationship between the energy density and the relative density of the 18 as-built samples manufactured in the conditions shown in Table 2. Relative density was evaluated from the contrast of the OM images. OM images of the representative plots are shown in Fig. 1(b)–(e) for reference. This revealed that approximately 100–150 J/mm^3 is the optimal range of energy density, and lower or higher energy density results in poor relative density owing to the lack of fusion or gas pores, respectively. Accordingly, the microstructure and properties of the four samples manufactured at an energy density of 111 J/mm^3 (200 W × 600 mm/s) or 125 J/mm^3 (300 W × 800 mm/s) with a scan strategy of both 67° and 90° were characterized in detail.

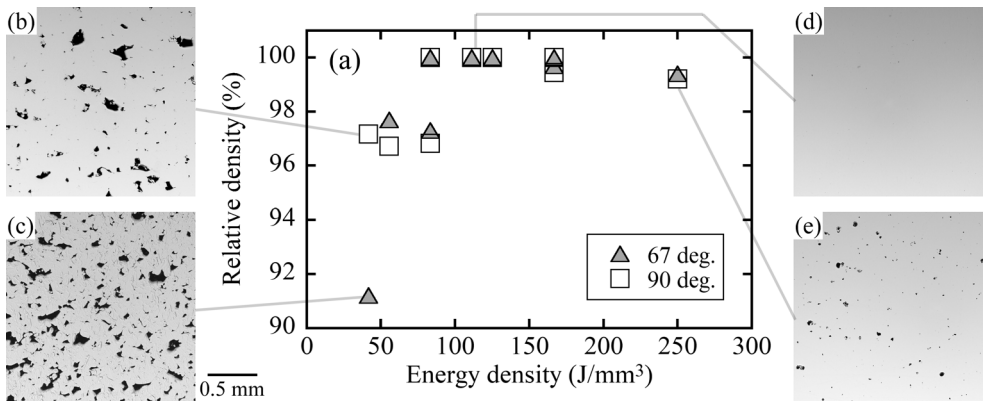

Figure 1: (a) Relationship between energy density and relative density of as-built LPBF samples. (b)-(e) optical micrographs of as-built samples used for evaluating the relative density.

Figure 2(a) shows an inverse pole figure (IPF) map overlaid on the image quality (IQ) map of the sample manufactured at 111 J/mm^3 × 90°. The build direction corresponds from the bottom to the top of the image. The normal orientation of the sample surface is represented in the figure. The stacking of parabolic-shaped coarse δ-ferrite grains was observed. In addition, fine martensite grains were distributed in the δ-ferrite matrix and a small amount of retained austenite phase was observed at the interface between δ-ferrite and martensite, as shown in Fig. 2(b) and (c). Furthermore, a strong texture of [001]//build direction and [001]//laser direction were observed, as shown in Fig. 2(d)–(f).

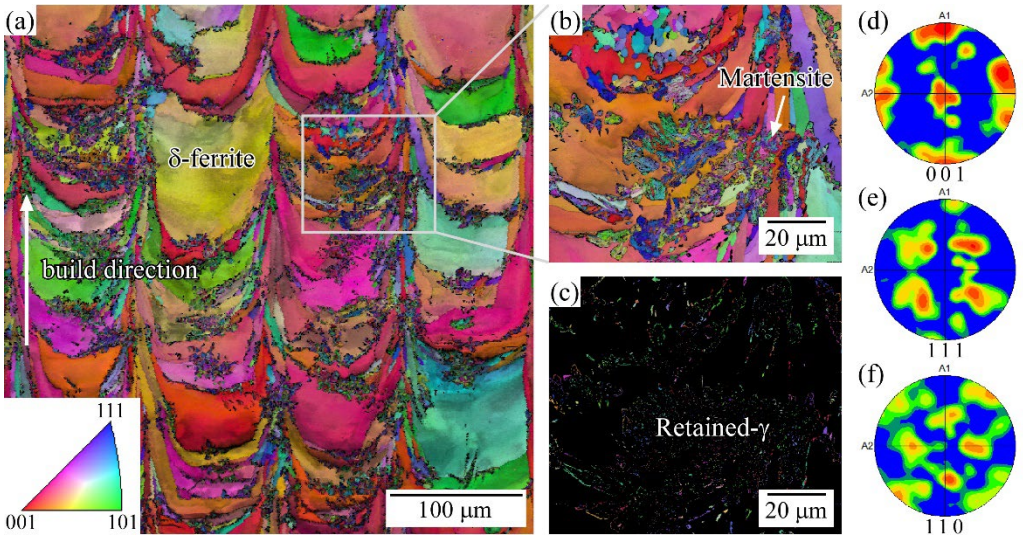

Figure 2: (a)–(c) IQ+IPF maps of as-built sample manufactured at 111 J/mm^3 × 90° and pole figure of (d) 001, (e) 111 and (f) 110.

Figure 3 schematically shows the formation mechanism of the duplex microstructure with δ-ferrite and martensite during the LPBF process. (a) Powder bed was prepared on a modified 9Cr-1Mo steel substrate. (b) When the laser is exposed on the powder bed, not only the melt pool (liquid phase) but also the heat-affected zone (HAZ) is generated on the substrate. When the temperature of the HAZ exceeds A_{c1} temperature, the substrate with the bcc structure (ferrite or martensite) should be transformed into the fcc structure. (c) After leaving the laser, significantly rapid solidification from the liquid results in the formation of columnar δ-ferrite grains at the melt pool [4] and the fcc grains that formed in the HAZ were transformed to martensite. (d)(e) The repetition of heating and cooling cycles during the LPBF process results in a duplex microstructure with δ-ferrite and martensite.

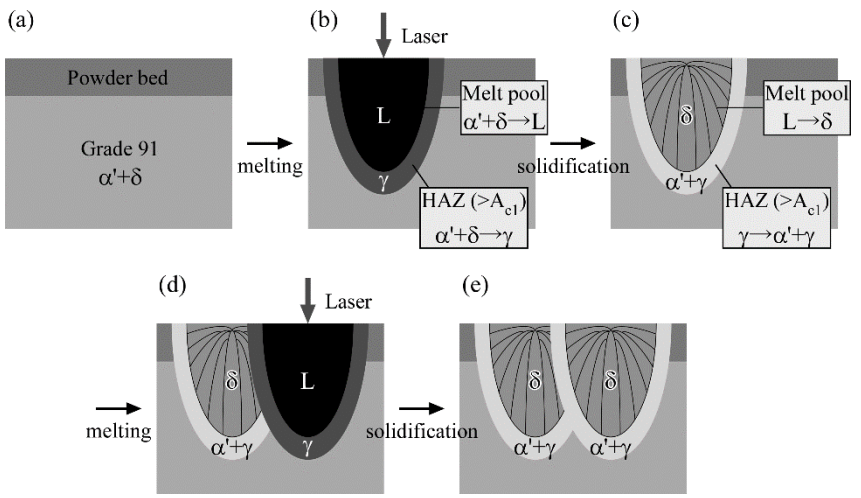

Figure 3: Microstructure formation mechanism during LPBF process.

Figure 4 shows the relationship between the energy density and the area fraction of δ-ferrite. A higher area fraction of δ-ferrite was obtained at a lower energy density, resulting from the smaller HAZ during the LPBF process. In addition, a 90° scan strategy resulted in a higher area fraction of δ-ferrite. As shown in Fig. 3(e), the HAZ overlapped with the neighboring melt pool in the same layer. In this case, solidified δ-ferrite and transformed martensite are overwritten to martensite and δ-ferrite, respectively. This interaction also occurs in the layer-by-layer determined by the geometry of laser scan strategy.

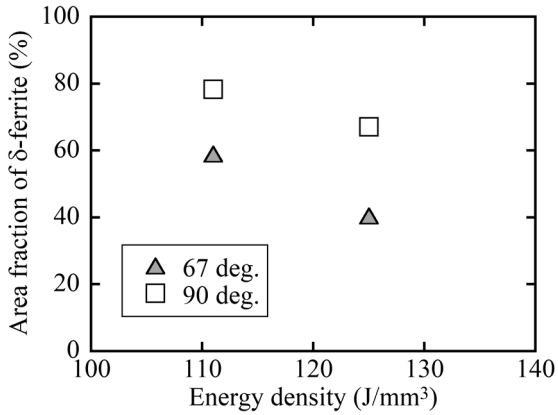

Figure 4: Relationship between energy density and area fraction of δ-ferrite.

Figure 5 shows the schematic of the rotation angle of laser scan in each layer. When the 90° scan strategy is selected, the laser passes through the same line on a x-y plane in every two layers. This geometry is preferable for the efficient overwriting of martensite to δ-ferrite. In contrast, the 67° scan strategy is preferable to preserve the martensite because the laser never passes through the same line on a x-y plane in the layer. This suggests that understanding this microstructure formation mechanism permits the control of the area fraction and distribution of δ-ferrite and martensite by optimizing the LPBF conditions.

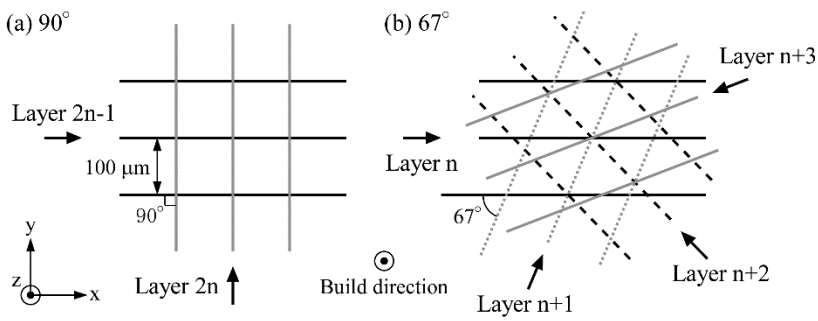

Figure 5: Schematics of the rotation angle of laser scan in each layer (scan strategy) of (a) 90° and (b) 67°.

Figure 6(a) shows an IQ + IPF map of the sample manufactured at 111 J/mm^3 × 90° after normalized at 1323 K for 30 minutes and tempered at 1053 K for 60 minutes. As-built microstructure morphologies with columnar δ-ferrite grains was completely disappeared and typical tempered martensite microstructure was obtained.

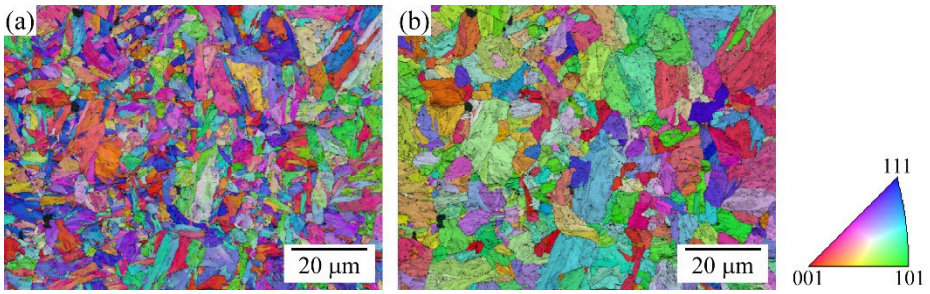

Figure 6: (a) IQ + IPF map of NT sample manufactured at 111 J/mm3 × 90° and (b) IQ + IPF map of prior austenite grains whose orientation was reconstructed by the Kurdjumov-Sachs orientation relationship.

Figure 6(b) shows the IQ + IPF maps of prior austenite grains whose orientation was reconstructed by considering the Kurdjumov-Sachs orientation relationship using OIM-Analysis 8.6 software. Based on this analysis, the prior austenite grain size was evaluated and plotted as a function of the area fraction of δ-ferrite, as shown in Fig. 7. This reveals that the prior austenite grain size increased with the area fraction of δ-ferrite in the as-built sample. This is resulting from the faster phase transformation kinetics of martensite than that of δ-ferrite during the normalization process. In other words, the prior austenite grain size could be controlled by optimizing the area fraction of δ-ferrite and martensite in the as-built microstructure.

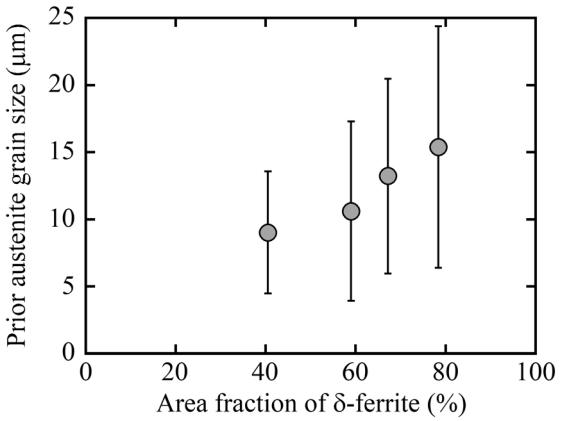

Figure 7: Relationship between area fraction of delta ferrite and prior austenite grain size.

Figure 8 shows the relationship between the area fraction of δ-ferrite and Vickers hardness of the as-built and NT samples. The Vickers hardness of the as-built samples was significantly higher than that of conventional modified 9Cr-1Mo steels (~230 HV) [5] and close to that of as-quenched

modified 9Cr-1Mo steel (~400 HV) [6]. The hardness is reduced with the area fraction of δ-ferrite, suggesting that a higher dislocation density in martensite contributes to the hardness. The hardness of the NT sample was reduced to the same level as that of conventional modified 9Cr-1Mo steels (~230) [5], and the effect of the building condition was smaller. Nevertheless, the hardness has a slightly negative tendency against the area fraction of δ-ferrite in the as-built sample, suggesting that a smaller prior austenite grain size results in higher hardness.

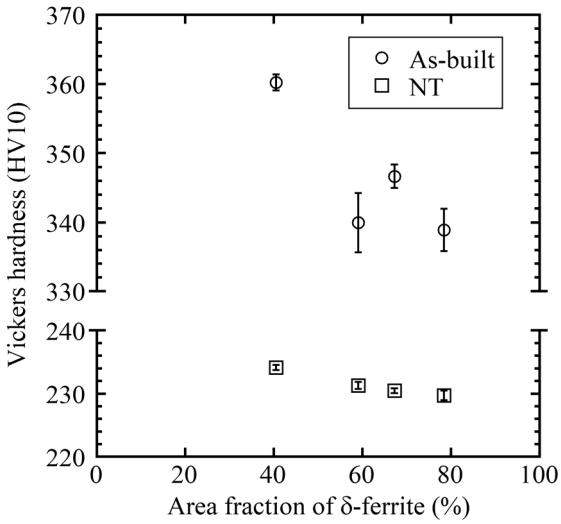

Figure 8: Vickers hardness of as-built and NT sample as a function of area fraction of delta ferrite in the as-built sample.

CONCLUSIONS

Microstructure of modified 9Cr-1Mo steel manufactured via laser powder bed fusion was investigated and following conclusions were reached resulting from the research.

- 111–125 J/mm^3 was the optimal energy density for the manufacturing of modified 9Cr-1Mo steel by laser powder bed fusion.

- As-built steel was composed of duplex microstructure of coarse columnar δ-ferrite and fine martensite grains resulting from the complex thermal history during LPBF. The area fraction of two phases can be controlled by LPBF conditions.

- Typical as-built microstructure morphologies can be eliminated by the post heat treatment that inducing the martensite transformation.

ACKNOWLEDGMENTS

The authors thank Dr. Toru Hara, Ms. Yuka Hara, Ms. Akiko Nakamura in National Institute for Materials Science (NIMS) for their support with the microstructural observations. This work was supported by Japan Boiler Association and Chubu Electric Power.

REFERENCES

[1] F. Masuyama, Advances in Physical Metallurgy and Processing of Steels. History of Power Plants and Progress in Heat Resistant Steels., ISIJ International 41 (2001) 612–625. https://doi.org/10.2355/isijinternational.41.612.

[2] O. El-Atwani, B.P. Eftink, C.M. Cady, D.R. Coughlin, M.M. Schneider, S.A. Maloy, Enhanced mechanical properties of additive manufactured Grade 91 steel, Scr Mater 199 (2021) 113888. https://doi.org/10.1016/j.scriptamat.2021.113888.

[3] ASME, Boilar and Pressure Vessel Code, Section II-A, SA213/SA213M Grade T91 Type 1, 2019.

[4] F. Villaret, X. Boulnat, P. Aubry, J. Zollinger, D. Fabrègue, Y. de Carlan, Modelling of delta ferrite to austenite phase transformation kinetics in martensitic steels: Application to rapid cooling in additive manufacturing, Materialia (Oxf) 18 (2021) 101157. https://doi.org/10.1016/J.MTLA.2021.101157.

[5] K. Sawada, K. Sekido, K. Kimura, K. Arisue, M. Honda, N. Komai, N. Fukuzawa, T. Ueno, N. Shimohata, H. Nakatomi, K. Takagi, T. Kimura, K. Nomura, K. Kubushiro, Effect of initial microstructure on creep strength of ASME grade T91 steel, ISIJ International 60 (2020) 382–391. https://doi.org/10.2355/isijinternational.ISIJINT-2019-358.

[6] K. Watanabe, S. Ida, K. Yoshimi, Influence of Carbides Precipitated by Low-temperature Tempering on the Room-temperature Mechanical Properties of Grade 91 Steel, ISIJ International 62 (2022) ISIJINT-2022-213. https://doi.org/10.2355/isijinternational.ISIJINT-2022-213.